Available online at www.sciencedirect.com
ScienceDirect
Journal of Photochemistry and Photobiology A: Chemistry 187 (2007) 72–77
Journal of Photochemistry and Photobiology A:Chemistry
www.elsevier.com/locate/jphotochem

Characterization and evaluation of fibrous $SrTiO_3$ prepared by hydrothermal process for the destruction of NO

Jinshu Wang [a,b,*], Shu Yin [b], Tsugio Sato [b]

[a] School of Materials Science and Engineering, Beijing University of Technology, Beijing 100022, China
[b] Division of Advanced System, Institute of Multidisciplinary Research for Advanced Materials, Tohoku University, Sendai 980-8577, Japan

Received 16 March 2006; received in revised form 14 August 2006; accepted 28 September 2006
Available online 6 October 2006

Abstract

Fibrous $SrTiO_3$ particles were prepared by a hydrothermal reaction method using strontium hydroxide octahydrate and protonic layered tetratitanate as raw materials. The samples were characterized by X-ray diffraction, X-ray photoelectron spectrometer, scanning electron microscopy, nitrogen adsorption–desorption isotherm measurements and diffusion reflectance spectra. $SrTiO_3$ existed as two different morphologies of particles, i.e., fibrous particles and nanosized particles which attached to the surface of former ones. $SrTiO_3$ seemed to be formed by two different ways. One way is a direct reaction between $H_2Ti_4O_9$ and $Sr(OH)_2$ and the other is a two-step reaction involving transformation of $H_2Ti_4O_9$ to monoclinic TiO_2 followed by a reaction with $Sr(OH)_2$. Fibrous nitrogen doped $SrTiO_3$, which exhibited excellent visible light responsive photocatalytic activity, was prepared by the heat treatment of fibrous $SrTiO_3$ under the flow of ammonia gas at 600 °C for 3 h. Under the irradiation of light with wavelengths larger than 400 and 290 nm, the photocatalytic activities of fibrous $SrTiO_3$ were 2.4 and 1.3 times greater than those of spherical $SrTiO_3$ prepared by the solid-state reaction.

Keywords: Photocatalytic activity; Fibrous $SrTiO_3$; Hydrothermal treatment; Nitrogen monoxide elimination

1. Introduction

The photocatalytic elimination of pollutants in water and air has attracted much interest around the world. Strontium titanate ($SrTiO_3$) is an important material which has applications in the photocatalysis and electronics industries [1–7]. There have been many synthesis methods applied to prepare $SrTiO_3$ powders including co-precipitation [8,9], hydrothermal synthesis [10–12], mechanochemical reaction [13,14], and combustion-synthesis [15]. These reports focused on the preparation of $SrTiO_3$ powders possessing a spherical shape. It was reported that powders constituting of special shapes such as fibers could be used for producing textured ceramics with enhanced dielectric properties, photocatalytic activity, etc. [16–18].

The photocatalytic properties of $SrTiO_3$ have been investigated in the past. The redox potential of electrons and holes induced by photo-irradiation is powerful enough to decompose hazardous pollutants [4,5] and to cleave H_2O into H_2 and O_2 gases [6]. However, these reports focused on using UV light, which is less than 5% of the solar beams on the earth, because of the relatively large band gap energy of 3.2 eV of $SrTiO_3$. We have prepared nitrogen doped $SrTiO_3$ by mechanochemical reaction and found that this kind of compound exhibited good visible light photocatalytic activity [19]. So, we prepared fibrous $SrTiO_3$ and fibrous nitrogen doped $SrTiO_3$ and evaluated the photocatalytic activities of these compounds by measuring the destruction capability of nitrogen monoxide.

2. Experimental

2.1. Sample preparation

The mixture of $H_2Ti_4O_9$ and $Sr(OH)_2{\cdot}8H_2O$ (Kanto Chem. Co., Japan) with a $Sr(OH)_2/H_2Ti_4O_9$ molar ratio of 15 was put into a Teflon-lined, sealed stainless vessel of internal volume of 20 cm^3. After raising the temperature to 225 °C, it was held at the temperature for 1 day under autogenous pressure. The product was washed with hydrochloric acid to remove excess $Sr(OH)_2$, then washed with deionized water three times and dried

* Corresponding author. Tel.: +86 10 67391101.
E-mail address: wangjsh@bjut.edu.cn (J. Wang).

1010-6030/$ – see front matter © 2006 Elsevier B.V. All rights reserved.
doi:10.1016/j.jphotochem.2006.09.012

overnight in a vacuum at 60 °C. In order to dope nitrogen, $SrTiO_3$ prepared by this method was calcined in an NH_3 atmosphere at 600 °C for 3 h. For comparison, a mixture of TiO_2 and $SrCO_3$ with the same molar ratio was heated at 1100 °C for 2 h for preparing spherical $SrTiO_3$ powders.

2.2. Catalyst characterization

X-ray diffraction (XRD) patterns were obtained using Cu Kα radiation (Shimadzu XD-D1). Specific surface areas (BET), Barrett–Joyner–Halenda (BJH) pore distribution and pore parameters of the powder samples were determined by nitrogen adsorption–desorption isotherm measurements at 77 K (Quantachrome NOVA 1000-TS). The binding energies of Sr, Ti, N and O were measured at room temperature using an electron spectromer (Perkin Elmer PHI 5600). The peak positions of each element were corrected by using that of C1s (284.6 eV). The particle size and shape were evaluated by a scanning electron microscope (Hitachi 2000) and transmission electron microscope (JEM-2000EX).

2.3. Photocatalytic activity measurement

The sample was placed in a hollow place of 20 mm × 15 mm × 0.5 mm on a glass holder plate and set in the center of the reactor (373 cm^3). The gas containing 1 ppm NO and 50 vol.% air (balance N_2) was passed at the flow rate of 200 cm^3 min^{-1}. A 450 W high pressure mercury arc was used as the light source for the photocatalytic reaction. The light wavelength was controlled by selecting filters, i.e., Pyrex glass for cutting off the light of $\lambda < 290$ nm and Kenko L41 Super Pro (W) filter <400 nm. The elimination of nitrogen monoxide was determined by measuring the concentration of NO gas at the outlet of the reactor using a NO_x analyzer (Yanaco, ECL-88A).

3. Results and discussion

Fig. 1 shows the X-ray diffraction patterns of starting material $H_2Ti_4O_9$ and hydrothermal products prepared under different conditions. It was found that single phase $SrTiO_3$ existed in the product after the hydrothermal reaction of $H_2Ti_4O_9$ and $Sr(OH)_2$ at 225 °C for 1 day (Fig. 1e).

Fig. 2 displays the SEM micrographs of (a) $H_2Ti_4O_9$ used as a starting material, (b)–(d) $SrTiO_3$ prepared by the hydrothermal reaction of $H_2Ti_4O_9$ and $Sr(OH)_2$ at 225 °C for 1 day with different magnifications and (e) TEM observation for $SrTiO_3$ powders made by the solid-state reaction. The hydrothermal product (Fig. 2b) retained the fibrous morphology of the starting material $H_2Ti_4O_9$ (Fig. 2a), and nanocrystals about 80–100 nm in diameter were observed on the surface of the fibrous $SrTiO_3$ particles, see Fig. 2c and d. On the other hand, $SrTiO_3$ produced by the conventional solid-state reaction of $SrCO_3$ and TiO_2 consisted of relatively large spherical particles of about 0.2–0.5 μm in diameter (see Fig. 2e).

Using $H_2Ti_4O_9$ and $Sr(OH)_2$ as the raw materials, $SrTiO_3$ seemed to be produced in the following two methods during hydrothermal process:

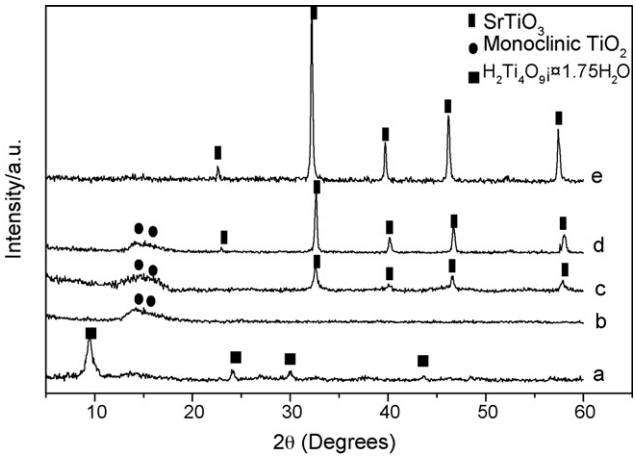

Fig. 1. XRD patterns of $H_2Ti_4O_9{\cdot}1.75H_2O$ before heat treatment (a) and after heating in water at 225 °C for 2 h (b), the reaction product by the hydrothermal reaction of $Sr(OH)_2$ and (b) at 225 °C for 2 h (c), the reaction products by the hydrothermal reaction of $H_2Ti_4O_9$ and $Sr(OH)_2$ at 225 °C for 2 h (d) and 1 day (e).

Method 1:

$$H_2Ti_4O_9 + 4Sr(OH)_2 \rightarrow 4SrTiO_3 + 5H_2O \quad (1)$$

Method 2 involved two steps as follows:

$$H_2Ti_4O_9 \rightarrow 4TiO_2 + H_2O \quad (2)$$

$$TiO_2 + Sr(OH)_2 \rightarrow SrTiO_3 + H_2O \quad (3)$$

Fig. 3a shows the idealized representation of the crystal structure of $H_2Ti_4O_9$. The basic framework is built up from a structure unit of four TiO_6 octahedral arrangement in a line by means of edge sharing. The units are combined with each other above and below to form a zigzag string sharing to make a staggered sheet. In method 1, Sr^{2+} ions might diffuse into the interlayer space and react with the TiO_6 octahedral layers of $H_2Ti_4O_9$ to form $SrTiO_3$ in situ. Since the protonic layered tetratitanate has relatively large innerlayer distance (0.90 nm), it is easy for Sr^{2+} ions (ionic radius 0.11 nm) to migrate into the crystal through the interlayer pathway and react with the TiO_6 octahedra layers. $SrTiO_3$ formed by this in situ reaction method retained the fibrous morphology of the starting material $H_2Ti_4O_9$. The nanocrystals on the surface of the fibrous $SrTiO_3$ particles might be formed by a dissolution–precipitation reaction mechanism. Since we added a large excess amount of $Sr(OH)_2$ in the raw material, the solution has high alkalinity. Therefore, the titanate partly dissolved in this alkaline solution to react with Sr^{2+} in the solution near the surface of the fibrous particles, leading to the formation of fine $SrTiO_3$ crystals on the surface of fibrous $SrTiO_3$ particles.

The second $SrTiO_3$ formation method should also be considered since we found that decreasing the hydrothermal treatment time from 1 day to 2 h, XRD patterns corresponding to the monoclinic TiO_2 and $SrTiO_3$ were found in the sample, see Fig. 1d, indicating that the monoclinic TiO_2 is an intermediate product during the formation of $SrTiO_3$. It is known that $H_2Ti_4O_9$ transforms into the monoclinic TiO_2 by the heat treatment. Fig. 1b shows that single phase monoclinic TiO_2

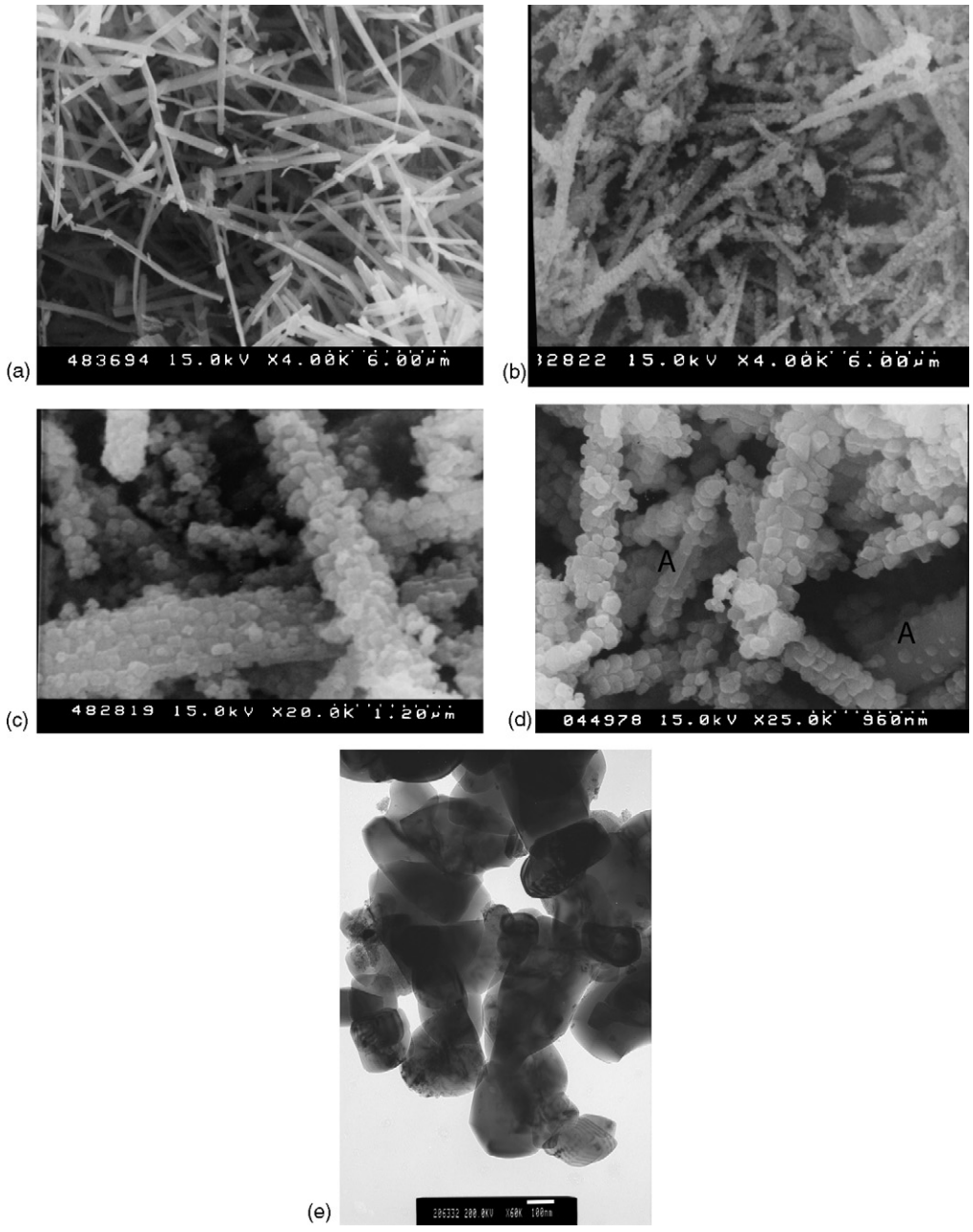

Fig. 2. SEM photographs of (a) $H_2Ti_4O_9{\cdot}1.75H_2O$, (b–d) $SrTiO_3$ prepared by the hydrothermal treatment of $H_2Ti_4O_9{\cdot}1.75H_2O$ and $Sr(OH)_2$ solution, and (e) TEM micrograph of $SrTiO_3$ prepared by the solid-state reaction of TiO_2 and $SrCO_3$.

can be formed by the hydrothermal treatment of $H_2Ti_4O_9$ in water for 2 h at 225 °C. Fig. 4 shows the micrographs of (a) the monoclinic TiO_2 prepared by the hydrothermal treatment of $H_2Ti_4O_9$ in water and (b) $SrTiO_3$ made with $Sr(OH)_2$ and the monoclinic TiO_2 under hydrothermal conditions. The monoclinic TiO_2 retained the fibrous morphology of the precursor but attached with fine crystals on the surface. Therefore, it seems that the monoclinic TiO_2 was also formed by two different mechanisms under the hydrothermal conditions. One is an in situ topotactic transformation reaction from layered tetratitanate to the monoclinic TiO_2 which retained the morphology of fibrous $H_2Ti_4O_9$. The other is a dissolution–reprecipitation reaction on the surface of the particles. Fig. 3b depicted the structure of the monoclinic TiO_2. The monoclinic TiO_2 is composed of corrugated sheets of edge- and corner-sharing TiO_6 octahedra, but the sheets are joined together to form a three-dimensional framework. So, it is relatively difficult for Sr^{2+} ions to migrate into the TiO_2 crystals to take the in situ reaction. As a consequence, the dissolution–precipitation reaction mechanism can be explained for the formation of $SrTiO_3$ when TiO_2 and $Sr(OH)_2$ are used as raw materials. Titanium oxide which dissolved in the alkaline solution quickly reacted with Sr^{2+} ions to precipitate $SrTiO_3$ on the fibrous particle. Consequently, the product $SrTiO_3$ still retained the morphology of the fibrous TiO_2 precursor.

In situ topotactic reaction between tetratitanate and Sr^{2+} ion can take place easily whereas the dissolution–precipitation

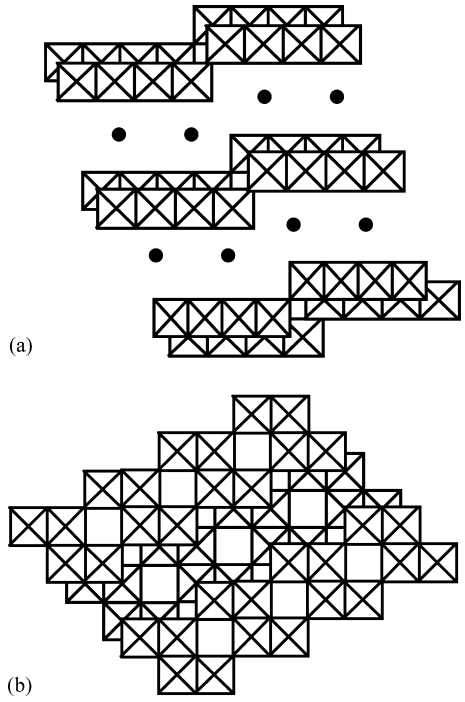

Fig. 3. The structure of (a) $H_2Ti_4O_9$ and (b) monoclinic TiO_2.

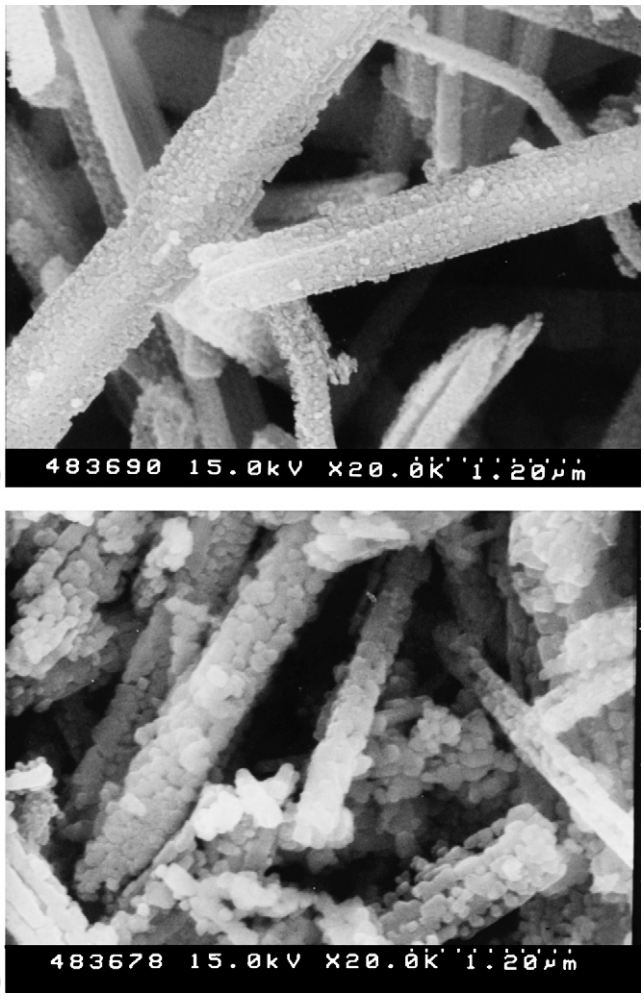

Fig. 4. SEM photographs of (a) the monoclinic TiO_2 prepared by the hydrothermal treatment of $H_2Ti_4O_9{\cdot}1.75H_2O$ at 225 °C for 2 h and (b) $SrTiO_3$ prepared by the hydrothermal treatment of TiO_2 in $Sr(OH)_2$ solution at 225 °C for 1 day.

reaction usually takes a long time. As shown in Fig. 1c and d, the intensity of $SrTiO_3$ made by hydrothermal treatment of $H_2Ti_4O_9$ and $Sr(OH)_2$ at 225 °C for 2 h is much higher than that prepared with TiO_2 and $Sr(OH)_2$ under the same hydrothermal treatment condition, indicating that the rate of the $SrTiO_3$ formation by the in situ reaction is much faster than that by a dissolution–precipitation reaction.

Based on the above discussion, we deduced that $SrTiO_3$ was formed through two different ways, topotactic reaction between tetratitanate and Sr^{2+} ion and the dissolution–precipitation reaction, and the reaction speed of the former one is higher than the latter one. $SrTiO_3$ formed through these two ways has the same morphology of fibrous particles. We also found that some $SrTiO_3$ fine particles dropped from the surface of the fibrous $SrTiO_3$ particles, leaving some spots with as smooth surface, see Fig. 2d (such as spot A). Since strontium hydroxide solution has relatively high alkalinity, grain boundary of $SrTiO_3$ was etched, as a result, the dissolved $SrTiO_3$ reprecipitated on the surface of fibrous particles as nanoparticles.

The nitrogen adsorption–desorption isotherms of the spherical $SrTiO_3$ prepared by the solid-state reaction and fibrous $SrTiO_3$ are shown in Fig. 5. In terms of shape, adsorption isotherms of both samples are classified as type IV with a hysteresis loop (IUPAC, 1985), which can be classified as type H2 indicating the presence of cylindrical capillaries with narrows and necks, with a certain contribution of "ink bottle" or bottle-type pores.

The pore size distributions (BJH) of these two samples are depicted in Fig. 6. Curve a corresponding to the spherical $SrTiO_3$ prepared by the solid-state reaction exhibited a narrow distribution with pore size family mainly located around 3 nm. On the other hand, fibrous $SrTiO_3$ has two pore size families located around 2 and 4 nm. As expected from the adsorption–desorption isotherm, fibrous $SrTiO_3$ gave a larger pore volume than spherical $SrTiO_3$ prepared by the solid-state reaction, i.e., their total pore volumes were 45.3 and 7.4 $cm^3\ g^{-1}$, respectively.

Miyauchi et al. report that N–H sites of the nitrogen doped TiO_2 surface act as acidic sites and nitrogen atoms play an important role in controlling the surface adsorptive properties [20]. Since adsorptive property is very important to determine the photocatalytic activities, we measured the change of NO concentrations in the presence of fibrous $SrTiO_3$ under the dark. It was found that the gaseous and adsorbed NO reached equilibrium in about 15 min. So, light illumination was initiated after 30 min to prevent the effect of adsorptive activity on the photocatalytic activity. Fig. 7 shows the time change of the concentration of NO in the presence of the spherical $SrTiO_3$ powders prepared by the conventional solid-state reaction (a), fibrous $SrTiO_3$ powders prepared by the hydrothermal reaction (b) and fibrous nitrogen doped $SrTiO_3$ prepared by the hydrothermal treatment followed by ammonia treatment at 600 °C for 3 h (c) under irradiating high pressure mercury arc with different light ranges ($\lambda > 400$ and 290 nm). It took about 10 min after photo-irradiation to reach

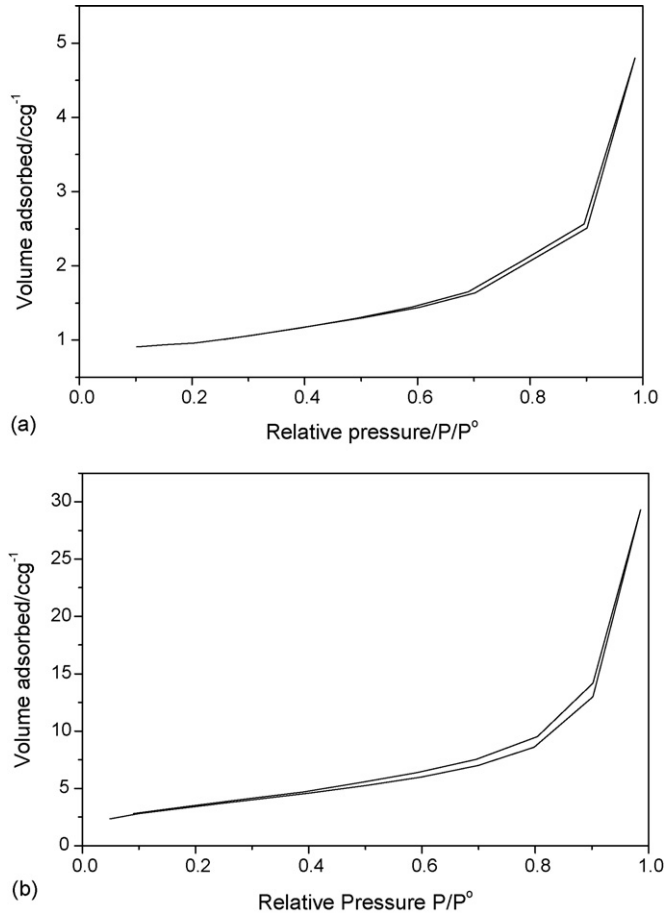

Fig. 5. Nitrogen adsorption–desorption isotherms for (a) spherical $SrTiO_3$ prepared by the solid-state reaction and (b) fibrous $SrTiO_3$ prepared by the hydrothermal treatment.

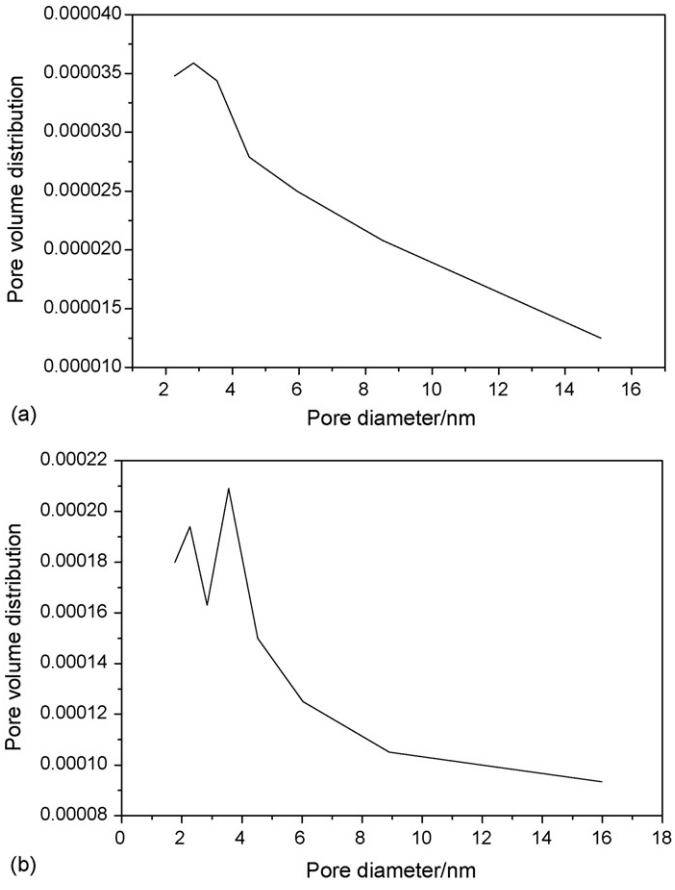

Fig. 6. Pore size distribution for (a) spherical $SrTiO_3$ prepared by the solid-state reaction and (b) fibrous $SrTiO_3$ prepared by the hydrothermal treatment.

the steady state concentration. When the light was turned off, NO concentration returned to its initial level of 1 ppm within 10 min. These results suggested that the light energy is necessary for the oxidation of NO, i.e., NO was photocatalytically eliminated. The fibrous $SrTiO_3$ exhibited higher NO elimination capability than the spherical $SrTiO_3$ by the solid-state reaction, see Fig. 7a and b. After nitrogen doping, the fibrous $SrTiO_3$ showed excellent photocatalytic activity, i.e., 39.9% NO could be eliminated under the irradiation of light $\lambda > 400$ nm, see Fig. 7c. The value was about 2.4 times higher than that with spherical $SrTiO_3$ powders. Furthermore, both fibrous nitrogen doped $SrTiO_3$ and un-doped $SrTiO_3$ exhibited better performance than spherical $SrTiO_3$ in the near ultraviolet light range ($\lambda > 290$ nm). Especially, the nitrogen doped one showed the highest NO destruction degree of 59.8%, which is about 1.3 times higher than that of a spherical one.

Fig. 8 shows the diffuse reflectance spectra of the spherical $SrTiO_3$ powder made by the solid-state reaction (a), fibrous $SrTiO_3$ prepared by the hydrothermal treatment (b) and fibrous nitrogen doped $SrTiO_3$ (c). Spherical $SrTiO_3$ showed an absorption edge at 390 nm corresponding to the band gap energy of 3.18 eV (see Fig. 8a), which was consistent with the band gap of 3.20 eV of $SrTiO_3$ reported by Cardona [21]. The fibrous $SrTiO_3$ showed a very slight shifting of the absorption edge to shorter wavelength, which might be due to the decrease of the crystallite size of $SrTiO_3$. After nitrogen doping, the optical absorption edge of $SrTiO_3$ red-shifted and the sample showed high visible light absorption, see Fig. 8c.

Fig. 9 shows XPS spectra of N1s of the fibrous nitrogen doped $SrTiO_3$. The nitrogen doped $SrTiO_3$ samples showed N1s peaks

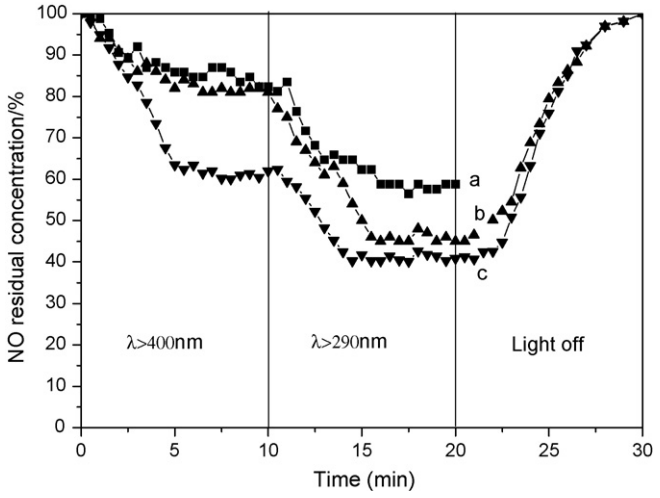

Fig. 7. Change in NO concentration under the irradiation of UV light in the presence of (a) spherical $SrTiO_3$ powder, (b) fibrous $SrTiO_3$ and (c) fibrous nitrogen doped $SrTiO_3$.

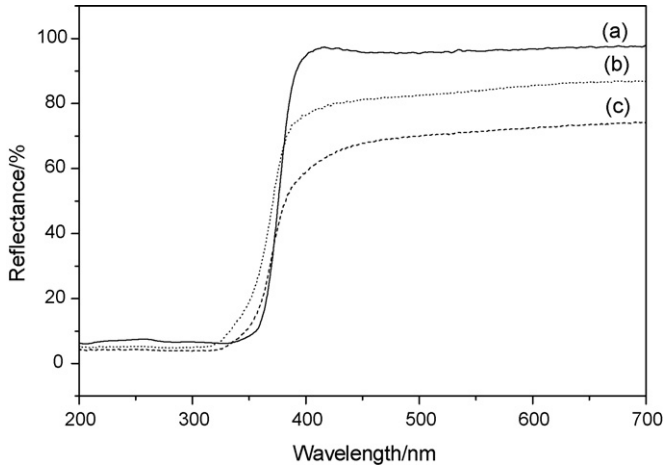

Fig. 8. The diffuse reflection spectra of (a) spherical $SrTiO_3$, (b) fibrous $SrTiO_3$ and (c) fibrous nitrogen doped $SrTiO_3$.

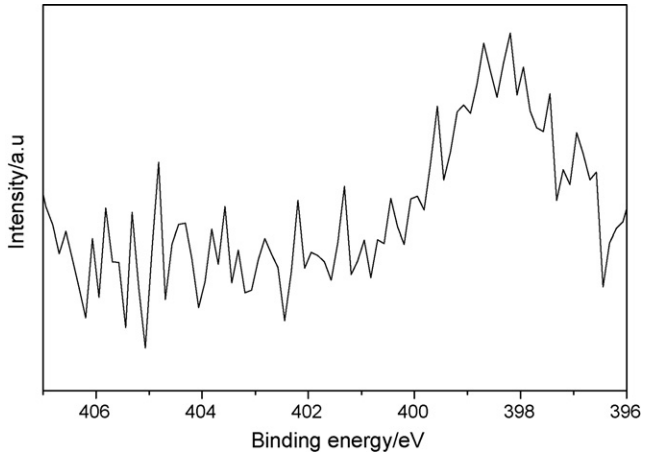

Fig. 9. XPS spectrum of N1s of the fibrous nitrogen doped $SrTiO_3$.

at about 398.5 eV assigned to the doping state of nitrogen, which agreed with our former result [19]. The concentration of all elements in the nitrogen doped $SrTiO_3$ samples were calculated from the XPS peak areas of individual elements through sensitivity factors for these elements. The atomic ratio of N/O was calculated as 0.01, indicating the formation of $SrTiO_{3-x}N_x$ with $x = 0.029$ by assuming that N had a substitutional fraction of $f_S = 1$. Therefore, nitrogen doping resulted in the improvement of photocatalytic activity of the sample.

Apart from the effect of nitrogen doping on the photocatalytic activity of the fibrous $SrTiO_3$, the higher specific surface area of the fibrous $SrTiO_3$ was the other main reason for its excellent NO elimination ability. The specific surface areas of the fibrous $SrTiO_3$ and fibrous nitrogen doped $SrTiO_3$ were 9.7 and 9.3 $m^2\ g^{-1}$, respectively, which was much higher than that of the spherical one (4.1 $m^2\ g^{-1}$). It is well known that as the particle size of the photocatalysts decrease, the ratio of the surface to the bulk increases. Therefore, the electron–hole pairs generated by absorbing light energy can quickly diffuse to the surface of the catalysts to form the active sites at which the redox reactions are induced. In addition, the larger specific surface area leads to higher adsorption ability of NO. As a result, the tendency for the recombination of photo-generated electrons and holes could be decreased with decreasing crystallite size. Furthermore, as shown in Fig. 5, the volume of mesopore, which was responsible for the effective adsorption of NO, in the fibrous $SrTiO_3$ was much larger than that of the spherical $SrTiO_3$ powders. Consequently, the fibrous $SrTiO_3$ prepared by the hydrothermal reaction which had a higher specific surface area and mesopore volume showed a higher ability for the destruction of NO.

4. Conclusions

(1) Fibrous strontium titanate particles attached nanocrystallites on the surface were obtained by the hydrothermal reaction of $Sr(OH)_2$ and $H_2Ti_4O_9$. The formation of these two kinds of particles can be explained by in situ topotactic reaction and dissolution–precipitation mechanism.

(2) The fibrous nitrogen doped $SrTiO_3$ formed by the hydrothermal reaction of $Sr(OH)_2$ and $H_2Ti_4O_9$ followed by the calcinations in ammonia atmosphere at 600 °C could eliminate 39.9% NO under the irradiation of light wavelength larger than 400 nm. The value was about 2.4 times greater than that of the spherical $SrTiO_3$ powder prepared by the solid-state reaction.

References

[1] H. Yukawa, K. Nakatsuka, M. Morinaga, Solid state Ionics 116 (1999) 89.
[2] Y. Guo, K. Kakimoto, H. Ohsato, Solid State Commun. 5 (2004) 279.
[3] P. Richard, H. Chang, D. Ellis, V. Dravid, J. Am. Ceram. Soc. 9 (1999) 2373.
[4] K. Domen, A. Kudo, T. Onishi, J. Catal. 102 (1986) 92.
[5] S. Ahuja, T.R.N. Kutty, J. Photochem. Photobiol. A: Chem. 97 (1996) 99.
[6] Q.S. Li, K. Domen, S. Naito, T. Onishi, K. Tamaru, Chem. Lett. 3 (1983) 321.
[7] K. Domen, S. Naito, T. Onishi, Chem. Phys. Lett. 4 (1982) 433.
[8] F. Perrot-Sipple, D. Aymes, J.C. Niepce, P. Perriat, Comptes Rendus de l'Académie des Sci., Series IIC: Chem. 7–8 (1999) 379.
[9] W.D. Yang, Mater. Sci. Eng. A 1–2 (1999) 148.
[10] M. Avudaithai, T.R.N. Kutty, Mater. Res. Bull. 5 (1987) 641.
[11] S. Zhang, Y. Han, B. Chen, X. Song, Mater. Lett. 4 (2001) 368.
[12] D. Chen, X. Jiao, M. Zhang, J. Eur. Ceram. Soc. 9 (2000) 1261.
[13] V. Berbenni, A. Marini, G. Bruni, J. Alloy Compd. 329 (2001) 230.
[14] T. Hungra, A.B. Hungra, A. Castro, J. Solid Chem. 177 (2004) 1559.
[15] J. Poth, R. Haberkorn, H.P. Beck, J. Eur. Ceram. Soc. 6 (2000) 707.
[16] Y. Ohara, K. Koumoto, H. Yanagida, J. Am. Ceram. Soc. 77 (1994) 2327.
[17] S. Yin, T. Sato, Ind. Eng. Chem. Res. 39 (2000) 4526.
[18] S. Yin, Y. Fujishiro, J. Wu, M. Aki, T. Sato, J. Mater. Process. Technol. 137 (2003) 45.
[19] J. Wang, S. Yin, M. Komatsu, Q. Zhang, F. Saito, T. Sato, Appl. Catal. B: Environ. 52 (2004) 11.
[20] M. Miyauchi, A. Ikezawa, H. Tobimatsu, H. Irie, K. Hashimoto, Phys. Chem. Chem. Phys. 6 (2004) 865.
[21] M. Cardona, Phys. Rev. 140 (1965) A651.